

Animating DDS Layers

One of the most powerful features of the DDS visualization technique is the ability to animate separate DDS layers. Watching an animated layer is quite impressive; the motion of the spots is highly salient and quickly attracts the attention of the viewer. In this section I describe the techniques for animating DDS layers as well as some observed benefits animation provides DDS.

The most effective style of animation I have used with DDS is to simply drift the underlying Gaussian sampling array across the surface, so that with each frame of the animation the Gaussian array shifts in position. Shifting the Gaussians before sampling the data variable means that with each new frame new data is sampled – if the amount of shift is less than the standard deviation of the Gaussians the visual effect is of the Gaussians sliding across the surface, revealing different areas in the data as they move.

This linear drift is implemented simply by adding a displacement to the texture coordinates used in the graphics system to display the Gaussians – because the Gaussian sampling array is treated as one texture, the entire Gaussian array moves as a unit, maintaining constant relative placement of the spots and the layer is coherent. In addition, because each Gaussian sampling array is toroidal and wraps around, there is no break or joint in the texture during the animation. The Gaussian sampling arrays are all functions of time, t , while the data function remains constant (equations 2.8 and 2.9).

$$\alpha_{tk}(i,j) = F_k(i,j) * G_{tk}(i,j), \quad 2.8$$

$$Accum_{tk}(i,j) = (1 - \alpha_{tk}(i,j)) * Accum_{tk-1}(i,j) + \alpha_{tk}(i,j) * C_k \quad 2.9$$

A Pendulum rocking motion, where the Gaussian sampling texture first translates to the right and then back to the left, similar to the motion of a swinging pendulum, provides an interesting, although less impressive, effect. I believe that the reason linear drift in one constant direction looks better than the pendulum rocking is because the rocking assigns two different directions and a varying speed to one layer. I believe DDS layers are visually separable because they are limited in the number of features each can display – one color, one size of spots, one layer depth, and one data variable per layer. Assigning one direction and a constant speed of motion to each layer works within this paradigm, whereas pendulum motion does not. In addition, if only one direction and speed of motion is assigned to a layer, then it is possible to assign other directions and or speeds of motion to more layers.

Animating other features of the DDS layer, such as the size of spots, has also been explored. In this experiment the size of one DDS spot layer was scaled from high to low and back to high following the pendulum swing motion. Whereas this provided a good illustration of how various sizes of spots show the underlying data variable quite differently, the overall effect of this type of animation was quite distracting, and certainly did not combine well with other animations.

One of the more interesting methods of animation I tried was to use the underlying data variable to set the speed of drift for each pixel in the Gaussian sampling array – where the data was high the texture would drift faster, where the variable was low, or zero, the texture would move slowly or not at all. With this method the Gaussian spots no longer moved as a coherent group across the surface, and instead created very distinct texture patterns in different regions in the data. This animation technique does not layer well and would be better suited for creating integrated type displays, described more in Chapter Four.

In my work I have observed several benefits to animating DDS layers, and most people viewing DDS animations remark on the power of animation. Animation of a DDS layer dramatically increases the visual salience of that layer; the viewer's attention is immediately drawn to the moving spots and the underlying data variable. DDS layers that are low in value, and therefore displayed with faint spots, become much easier to see. I have also noticed that small, spatially isolated areas that may go unnoticed become more salient with animation: the flickering on/off of color as the areas are alternately sampled and not sampled is quite noticeable.

One of the more exciting benefits of animation is that the moving Gaussians sample different points in the variable's spatial extent over time, so all data values are eventually sampled and displayed. The viewer is able to form a complete mental representation of the data while watching the animation. It is my opinion that animating DDS layers increases the visual salience so much, that it more than compensates for the loss of data through sampling, and because the data is seen in entirety over time, animated DDS layers may prove to be a better way of looking at data than non-sampled static images.

Several example animations are included on the CD provided with this dissertation. They are discussed further in Chapter Five: Future Work.

Visualization Gallery

Scanning Electron Microscope

The SEM data set is from the elemental decomposition of a geological sample. The data represents the distribution of eight base elements and a backscattering measurement. Grayscale images of all nine layers are presented in Figure 2.32. Three DDS images are presented: Figure 2.33 with three layers; Figure 2.34 with six layers; and Figure 2.35 with nine layers. Figure 2.36 presents an alternative mapping for the nine layers. The data presented here was given to our research group by EDAX, Inc. [EDAX, Inc., 2003].

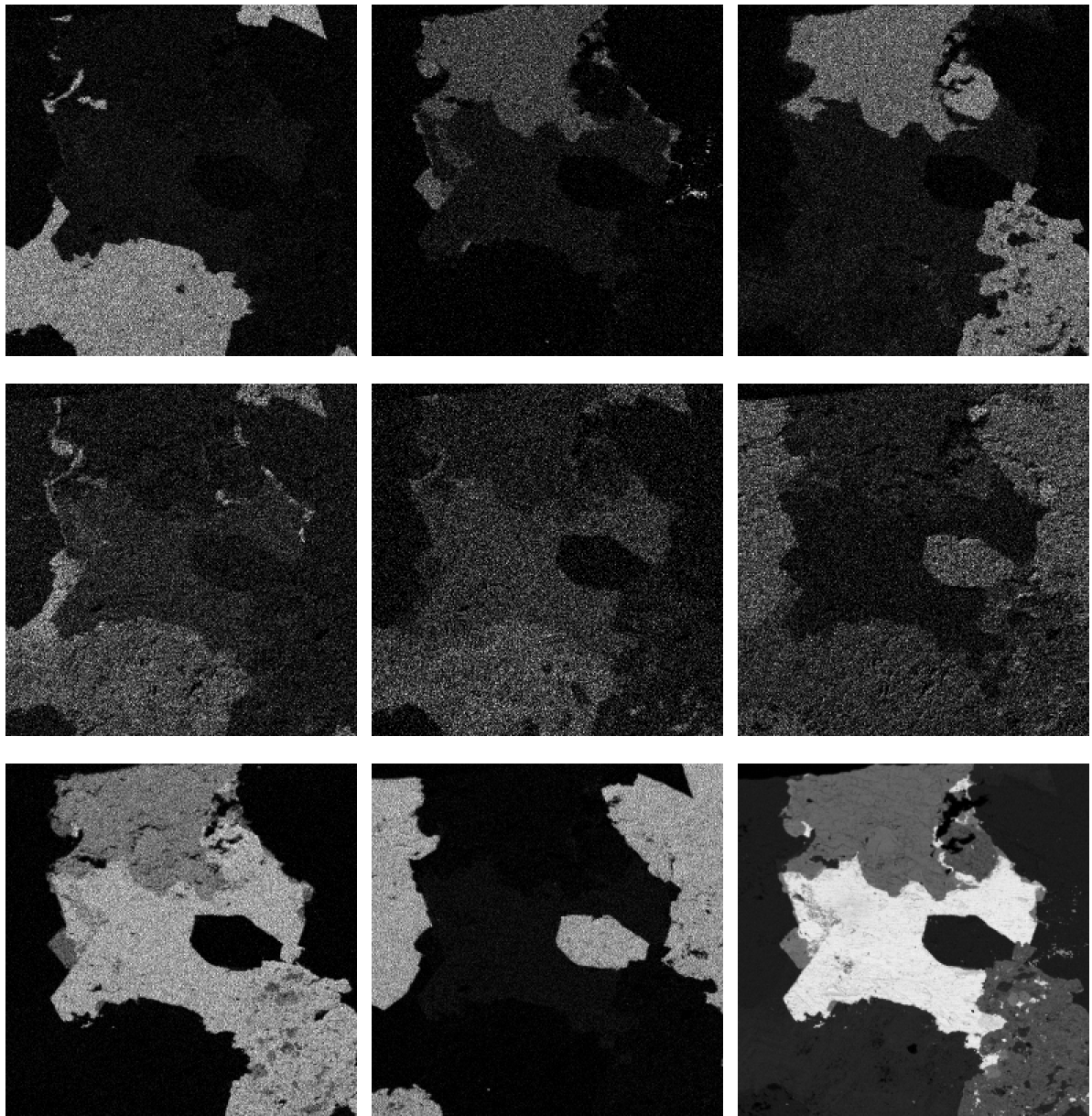


Figure 2.32: Grayscale images of the nine SEM variables. Top row: calcium, copper, iron. Middle row: oxygen, magnesium, manganese. Bottom row: sulfur, silicon, backscattering.

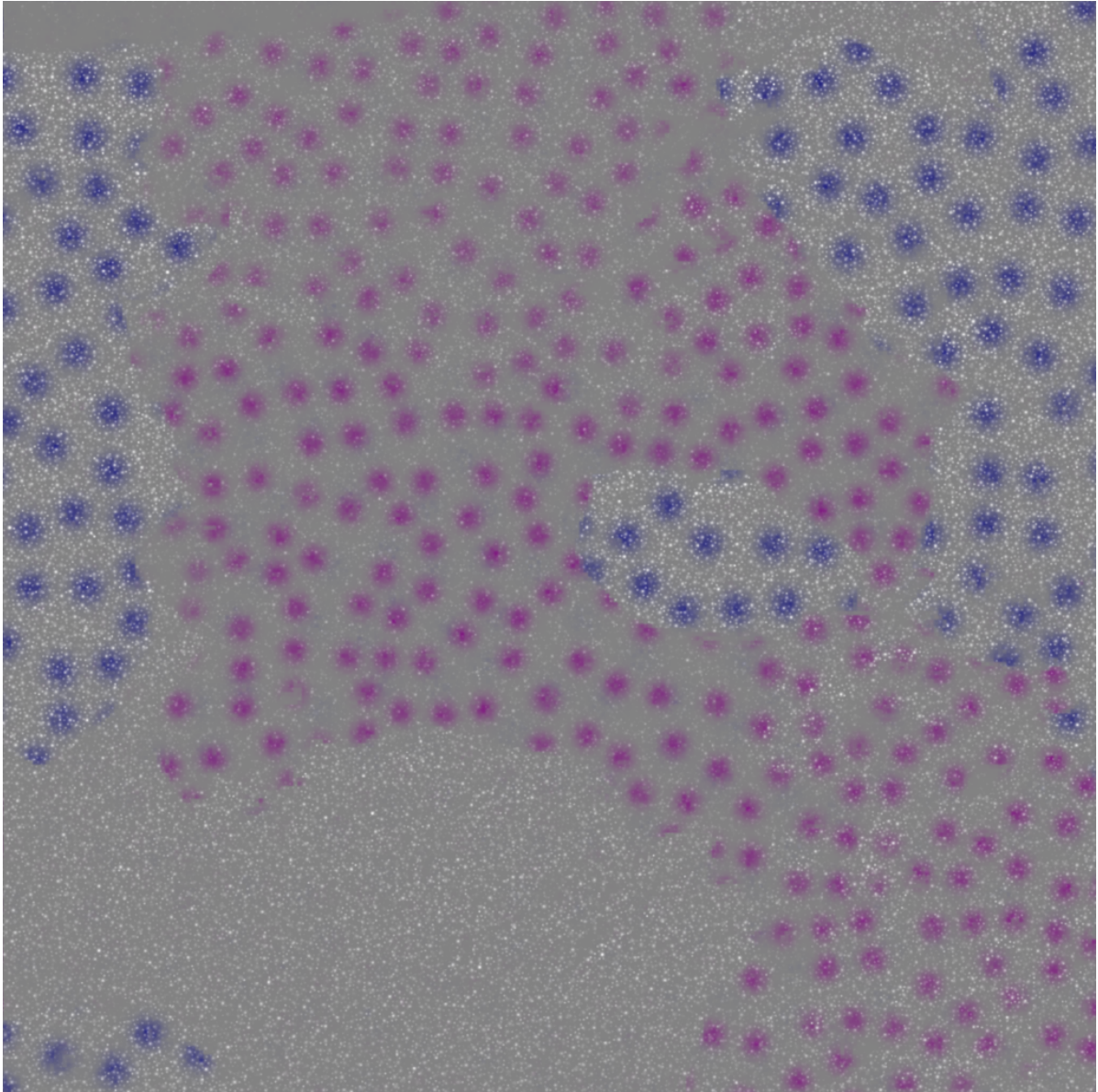


Figure 2.33: Three layers of the SEM data set: silicon in dark blue, sulfur in purple, and oxygen in white.

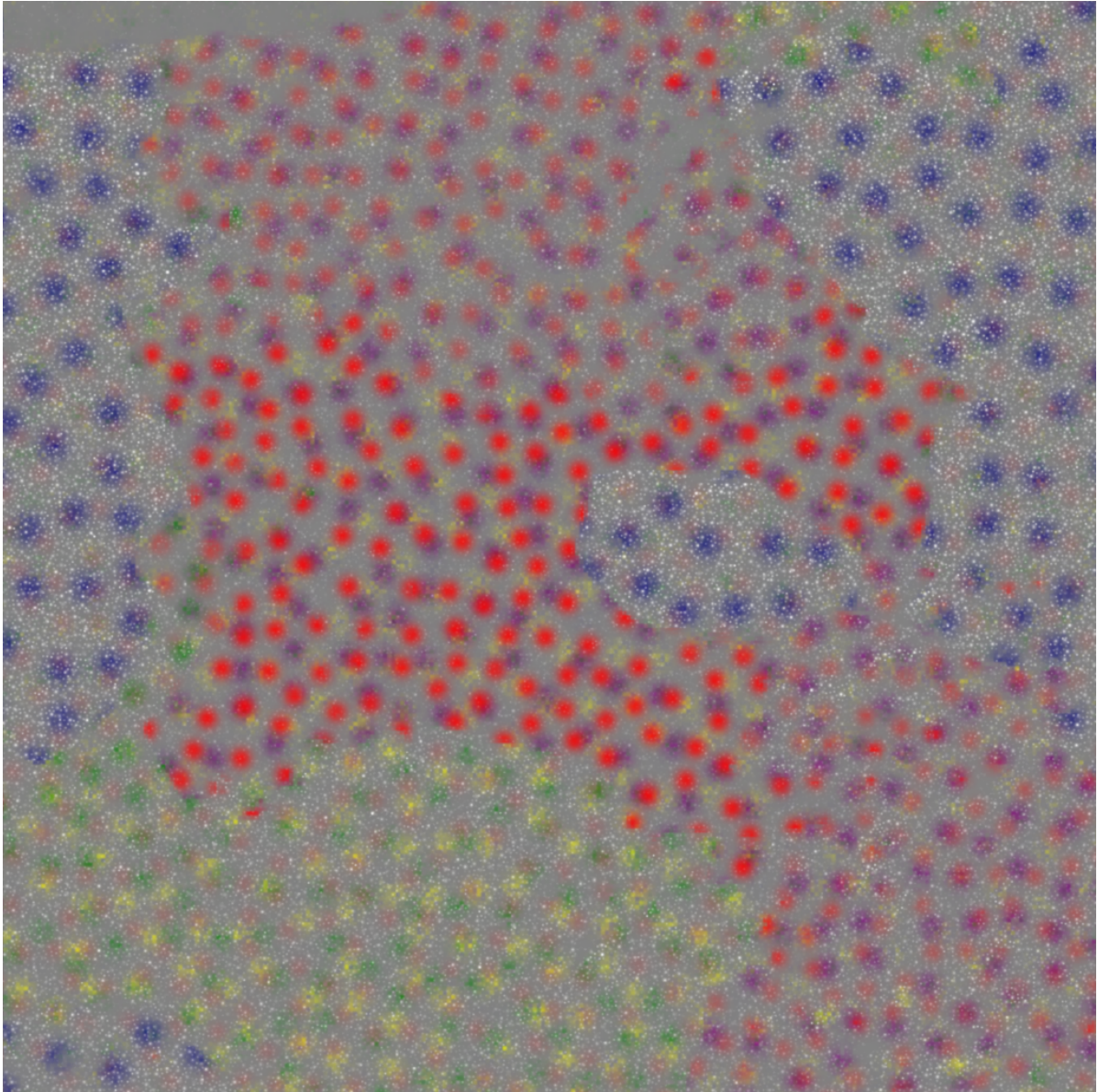


Figure 2.34: Six SEM layers. Three new layers added to Figure 2.33 are: magnesium in yellow, manganese in green, and the backscattering image in red.

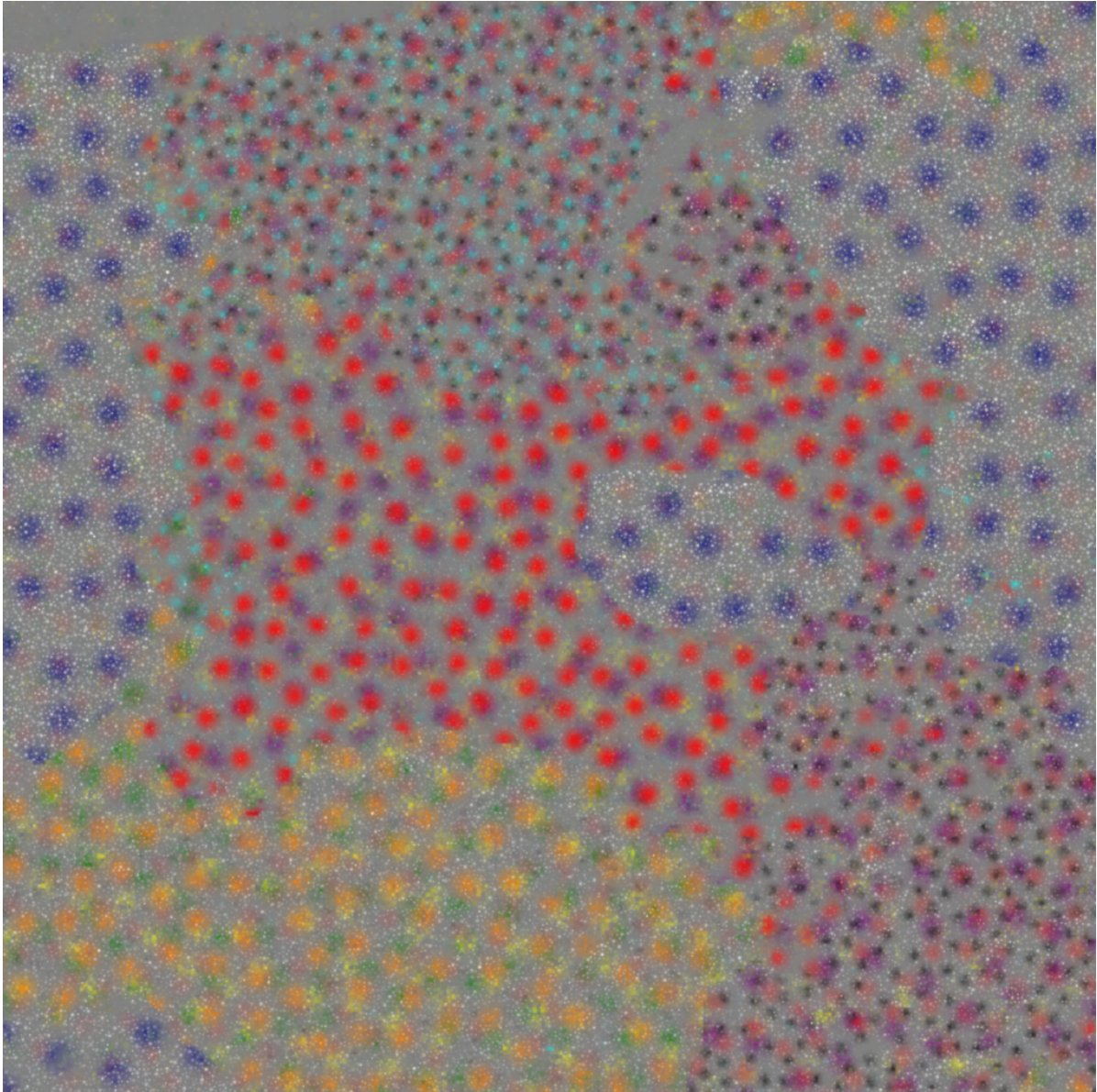


Figure 2.35: All nine SEM layers combined in one image. The three layers added to Figure 2.34 are: iron in black, copper in cyan, and calcium in orange. A tenth layer, repeating the white oxygen spots is also included.

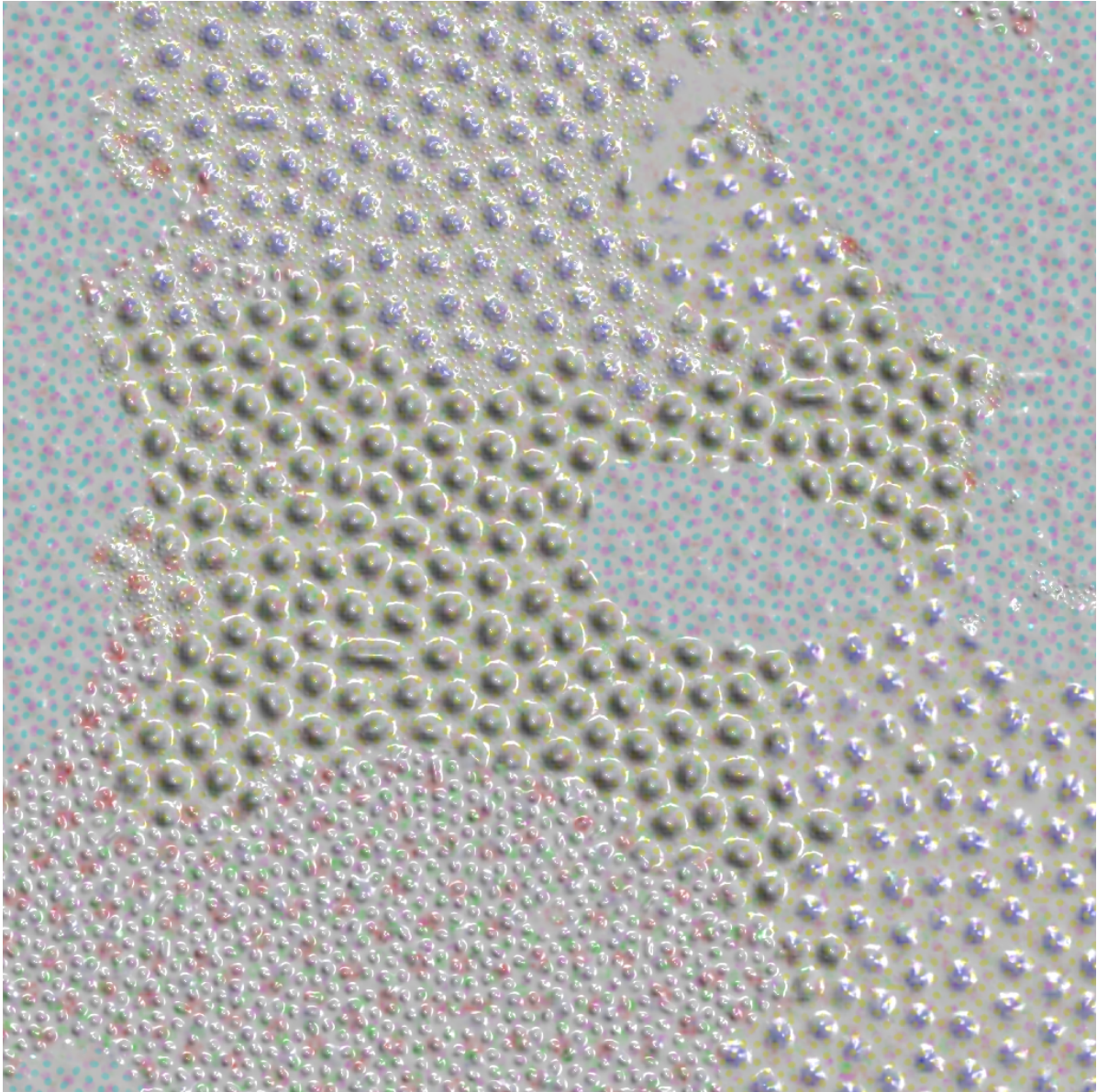


Figure 2.36: An alternative mapping of the SEM variables that has three bump layers: the backscattering image in large bumps, calcium in medium bumps, and copper in tiny bumps; and six color layers: iron in larger blue, sulfur in small yellow spots, silicon in small purple spots, oxygen in small cyan spots, magnesium in small green spots, and manganese in small red spots.

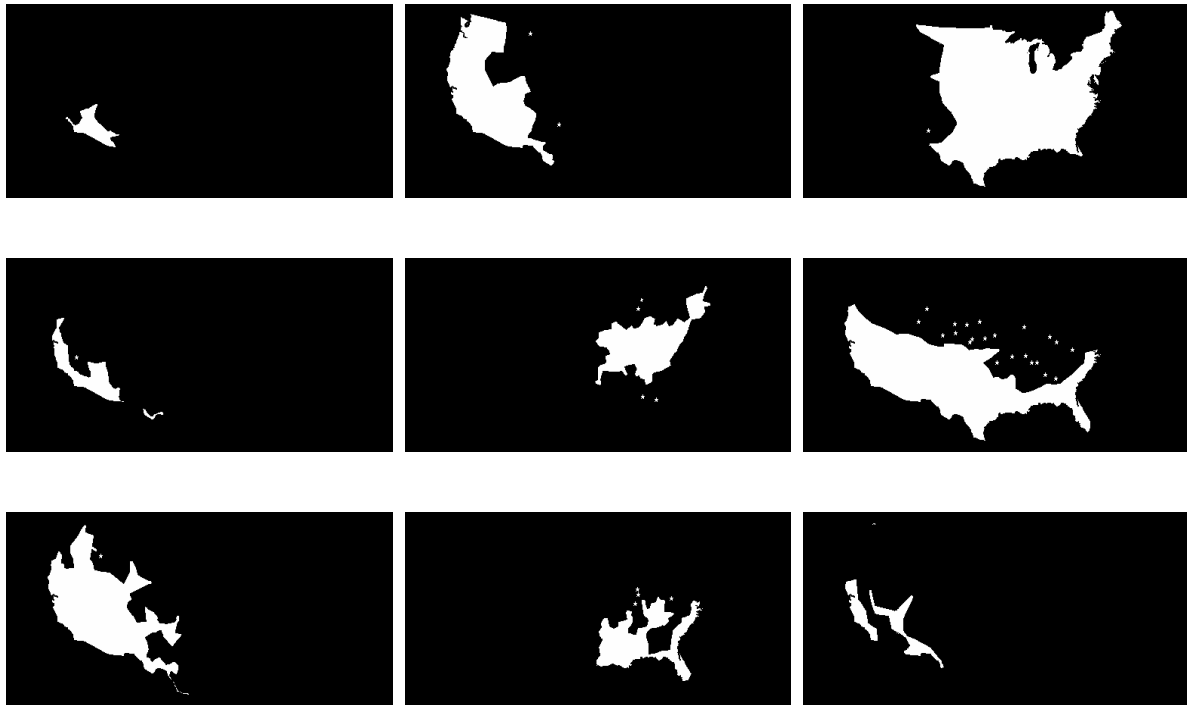


Figure 2.37: Bat habitat ranges for the following bat species: California leaf-nosed, California myotis, eastern red, greater bonneted, Indian myotis, Mexican free-tailed, pallid, rafinesque's big eared, and western red.

Bat Habitat Range

The bat habitat range data is from the National Atlas of the United States [2003]. Habitat ranges are binary in format, with values of 1 where the bats are found to live and 0 where they are not found. Figure 2.37 presents grayscale images for nine species of bat. Figures 2.38 through 2.40 present DDS images of the bat data.

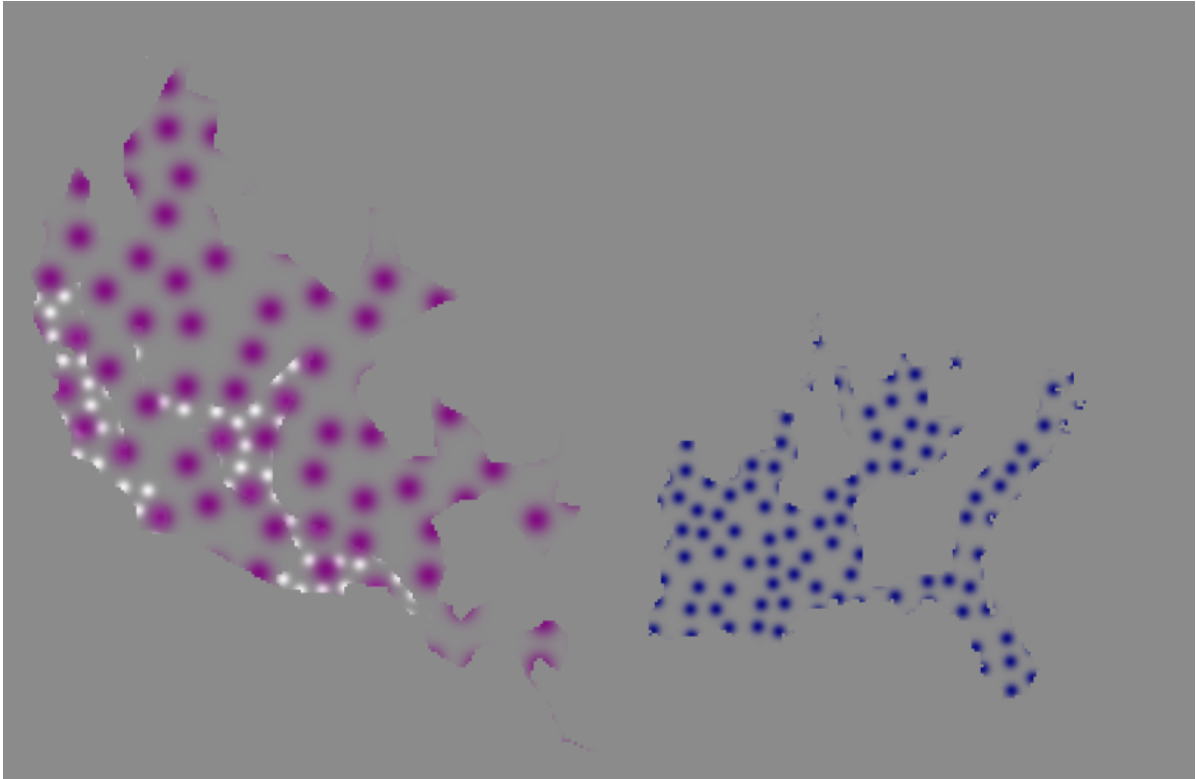


Figure 2.38: Three layers of the bat habitat data. The species shown are: western red in white, rafinesque's big-eared in dark blue, and the pallid bat in purple.

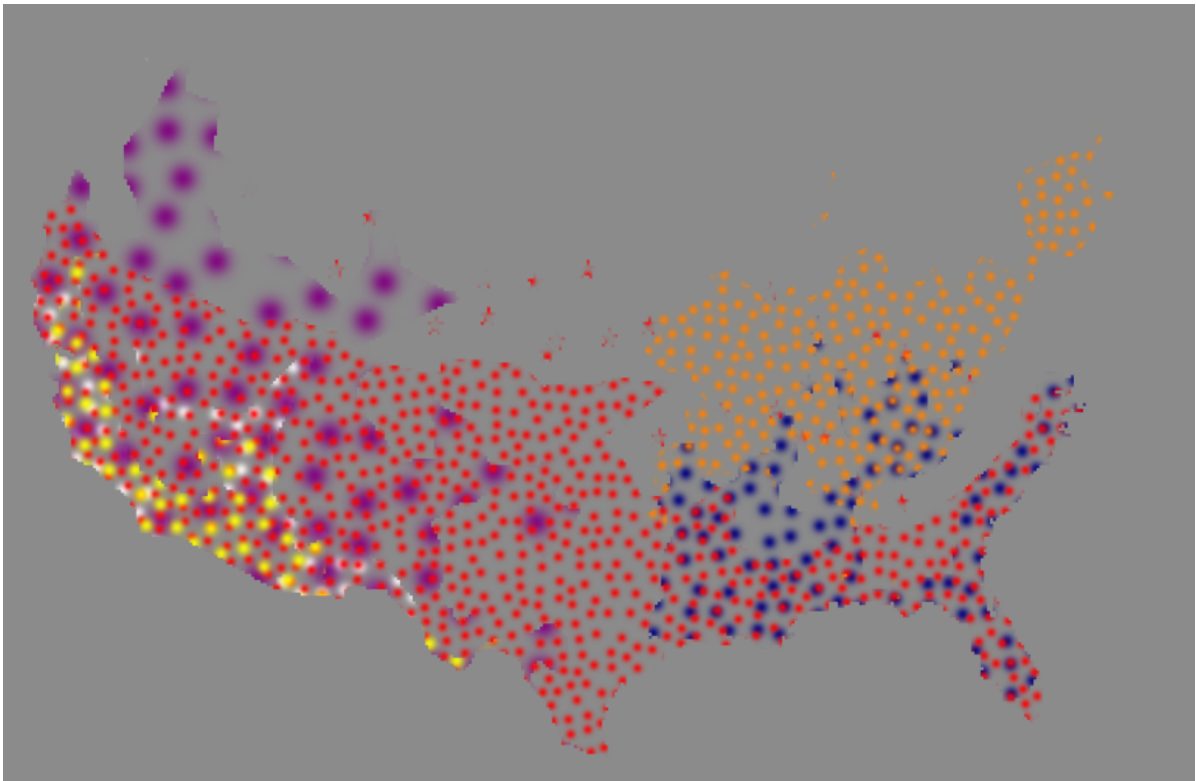


Figure 2.39: The habitat ranges of six species of bat are shown. Added to Figure 2.39 are: Mexican free-tailed, in red, Indian myotis in orange, and the greater bonneted bat in yellow.

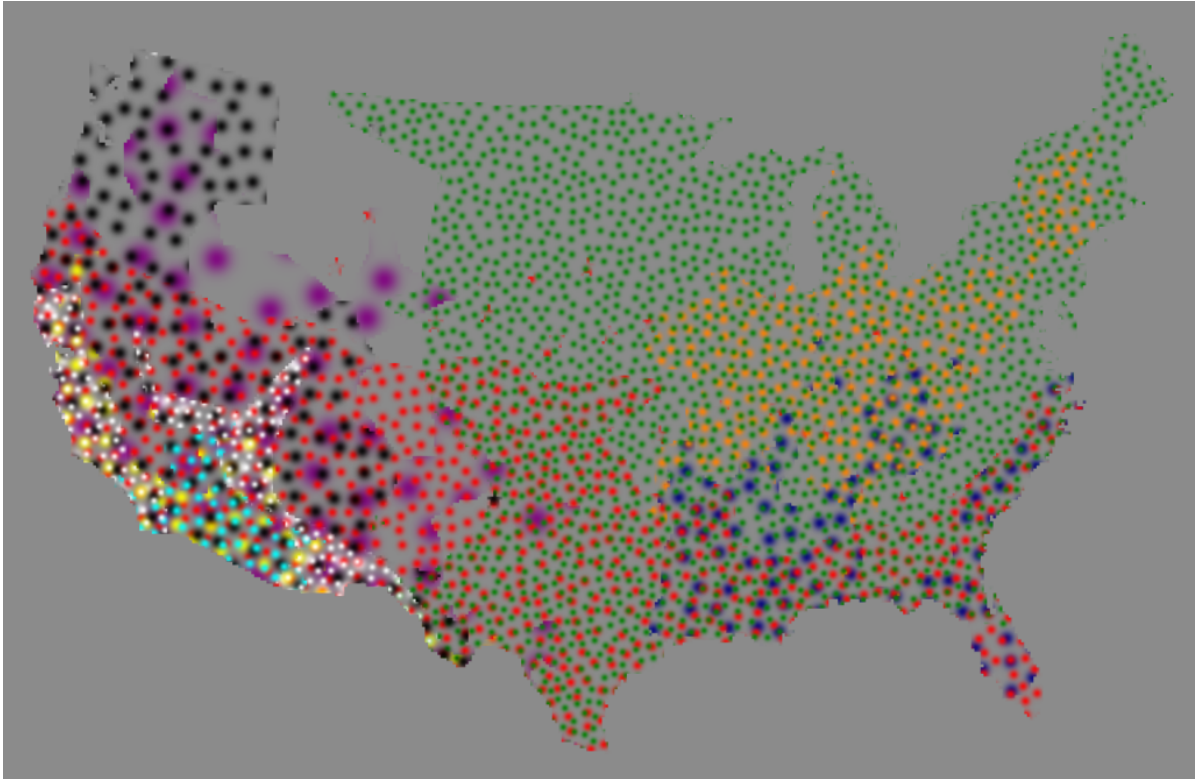


Figure 2.40: The habitats of nine bat species are shown. Added to Figure 2.40 are eastern red in green, California myotis in black, and California leaf-nose in cyan. A tenth layer for the western red bat, in smaller white spots, is added to improve the salience of the data.

Climate

Weather data from the Intergovernmental Panel on Climate Change [IPCC, 2003] is presented in Figures 2.41 through 2.50. Seven different variables are displayed: average cloud cover (percent), diurnal temperature range (degrees C), ground-frost frequency (days), precipitation (millimeters/day), radiation (W/square meter), vapor pressure (hPa), and wind speed (meters/second).

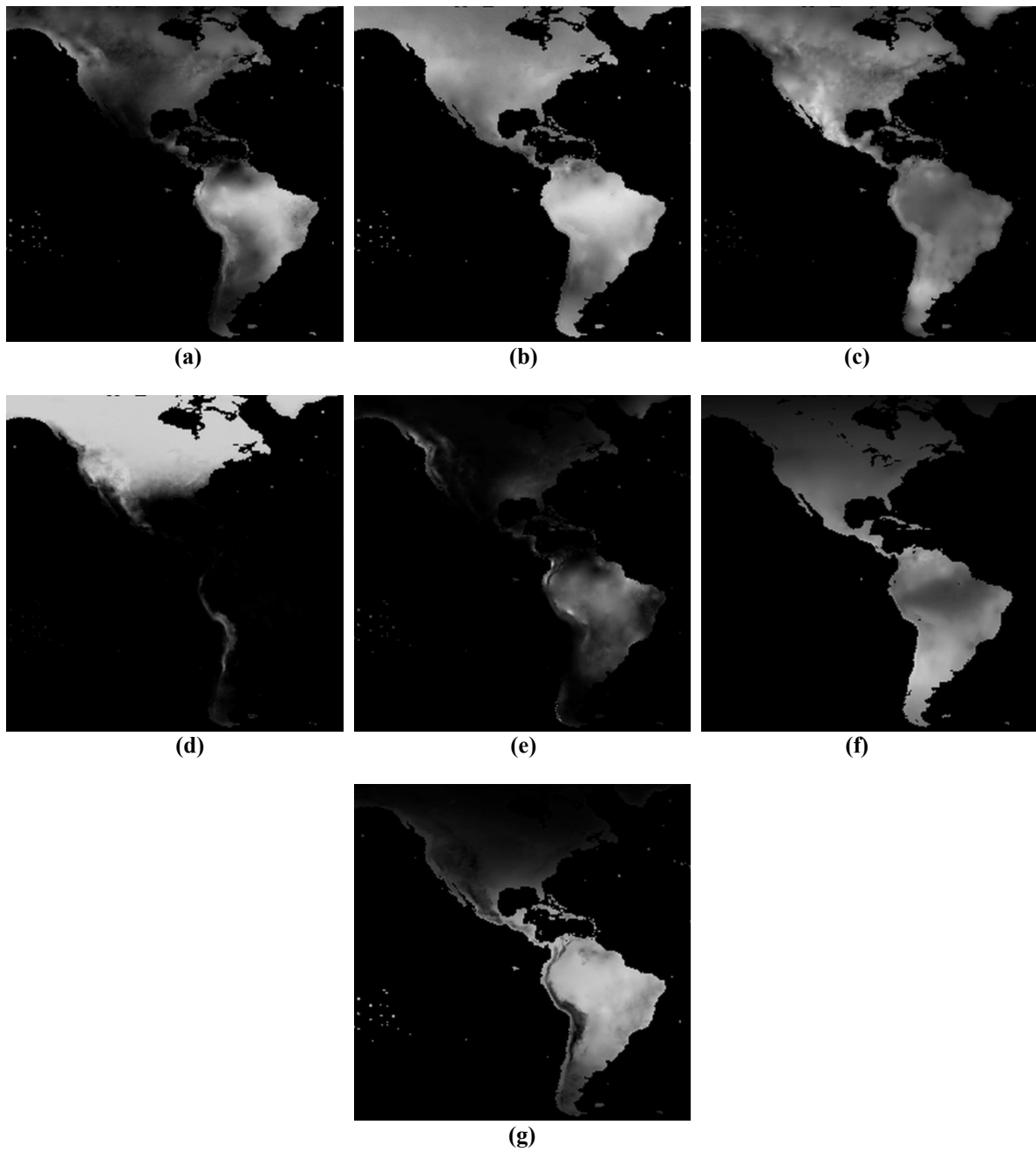


Figure 2.41: Climate data averages for the month of February, 1981-1990: wet-day frequency (days) in (a); cloud cover (percent) in (b); diurnal temperature range (degrees C) in (c); ground-frost frequency (days) in (d); precipitation (millimeters/day) in (e); radiation (W/square meter) in (f); vapor pressure (hPa) in (g).



Figure 2.42: DDS image of the climate data from February, 1981-1990: vapor pressure (hPa) in red spots and precipitation (millimeters/day) in blue spots.

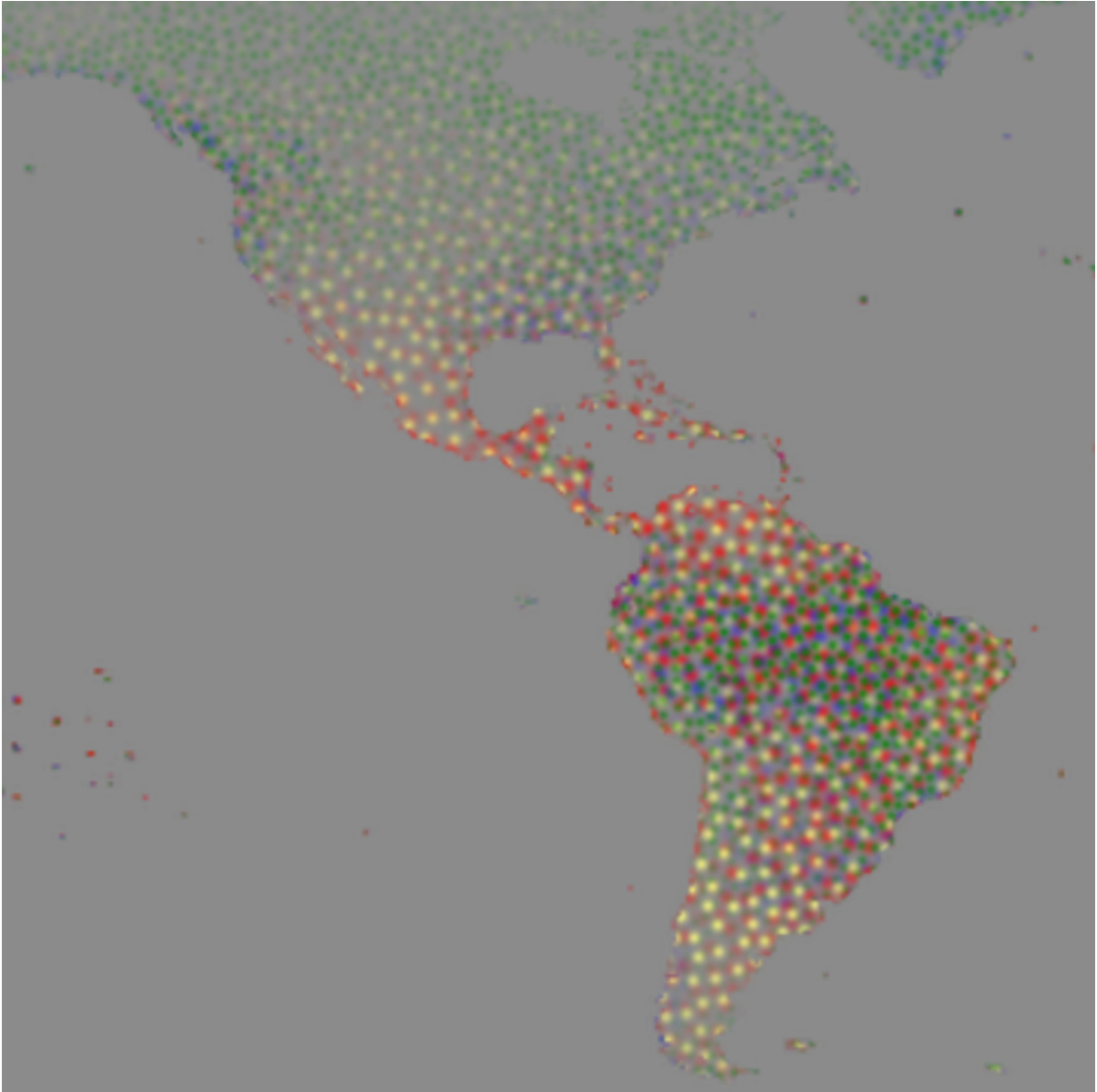


Figure 2.43: DDS image of the climate data from February, 1981-1990: vapor pressure (hPa) in red spots and precipitation (millimeters/day) in blue spots, wet-day frequency (days) in green spots, and radiation (W/square meter) in yellow spots.



Figure 2.44: DDS image of the climate data from February, 1981-1990: vapor pressure (hPa) in red spots and precipitation (millimeters/day) in blue spots, wet-day frequency (days) in green spots, and radiation (W/square meter) in yellow spots, ground-frost frequency (days) in white spots, and cloud cover (percent) in cyan spots.



Figure 2.45: DDS image of the climate data from February, 1981-1990: vapor pressure (hPa) in red spots, precipitation (millimeters/day) in blue spot, wet-day frequency (days) in green spots, radiation (W/square meter) in yellow spots, ground-frost frequency (days) in white spots, cloud cover (percent) in cyan spots, and diurnal temperature range (degrees C) in purple spots.

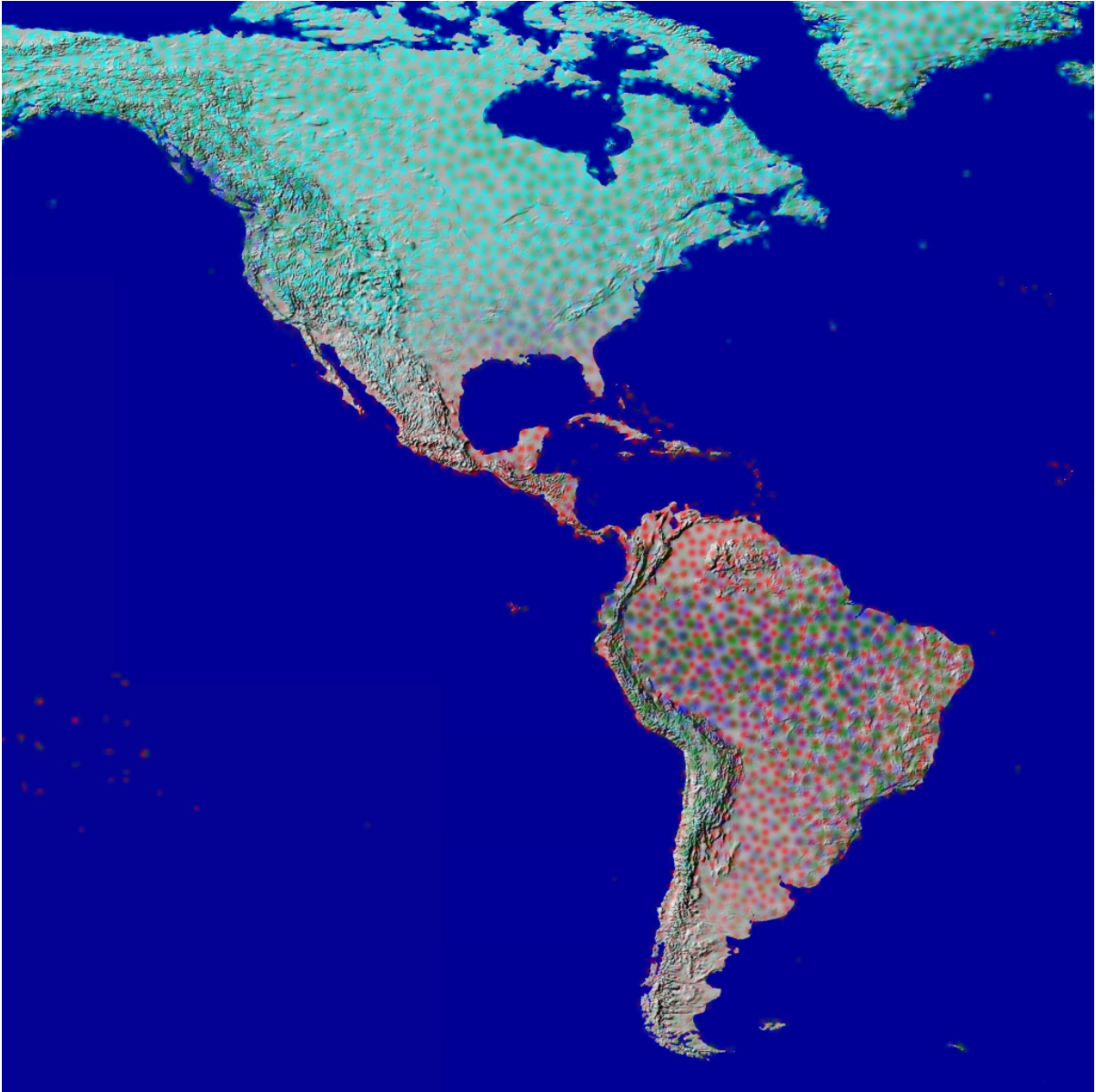


Figure 2.46: DDS image of the climate data from February, 1981-1990: vapor pressure (hPa) in red spots, precipitation (millimeters/day) in blue spot, wet-day frequency (days) in green spots, and ground-frost frequency (days) in cyan spots. In this example the spot layers are overlaid on a relief map.

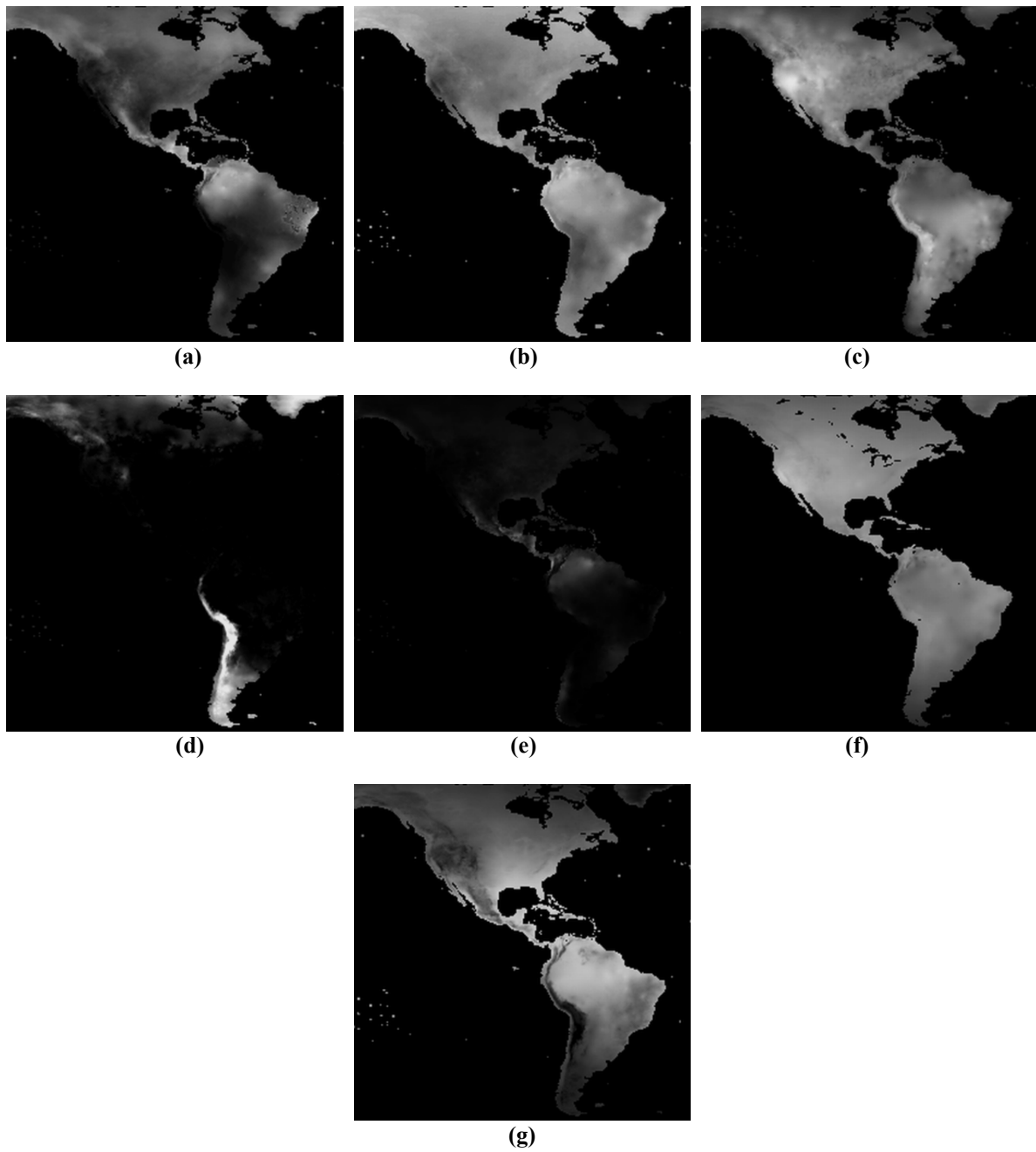


Figure 2.47: Climate data averages for the month of August, 1981-1990: wet-day frequency (days) in (a); cloud cover (percent) in (b); diurnal temperature range (degrees C) in (c); ground-frost frequency (days) in (d); precipitation (millimeters/day) in (e); radiation (W/square meter) in (f); vapor pressure (hPa) in (g).



Figure 2.48: DDS image of the climate data from February, 1981-1990: vapor pressure (hPa) in red spots, precipitation (millimeters/day) in blue spots, and wet-day frequency (days) in green spots.



Figure 2.49: DDS image of the climate data from February, 1981-1990: vapor pressure (hPa) in red spots, precipitation (millimeters/day) in blue spot, wet-day frequency (days) in green spots, radiation (W/square meter) in yellow spots, and ground-frost frequency (days) in white spots.



Figure 2.50: DDS image of the climate data from February, 1981-1990: vapor pressure (hPa) in red spots, precipitation (millimeters/day) in blue spot, wet-day frequency (days) in green spots, radiation (W/square meter) in yellow spots, ground-frost frequency (days) in white spots, cloud cover (percent) in cyan spots, diurnal temperature range (degrees C) in purple spots, and precipitation (millimeters/day) again in blue spots.

Photographs

Healey and Enns [2002] apply their painterly visualization technique to photographs as an artistic, non-photorealistic rendering technique. In their examples the photographs are separated into the red, green, and blue image components to represent three different data layers. This is an interesting technique that I have also tried with DDS. Figure 2.51 shows the process.

Three observations immediately come to mind: 1) saturation can be used to convey information, similar to intensity; 2) the images are darker than the original photograph – due to sparse sampling and the black background; 3) even though the three underlying color images are only displayed with red, green, and blue spots, the image colors are perceived correctly.

Illusions

It is interesting to consider perceptual illusions such as the Necker cube, the magic square, and the face-vase illusion (Figures 2.52 and 2.53). Perceptual illusions provide clues to human visual perception; if they are visible when displayed with DDS, then perhaps some of the same perceptual phenomena that describe how people see the illusions can be applied to how people see and understand DDS images.

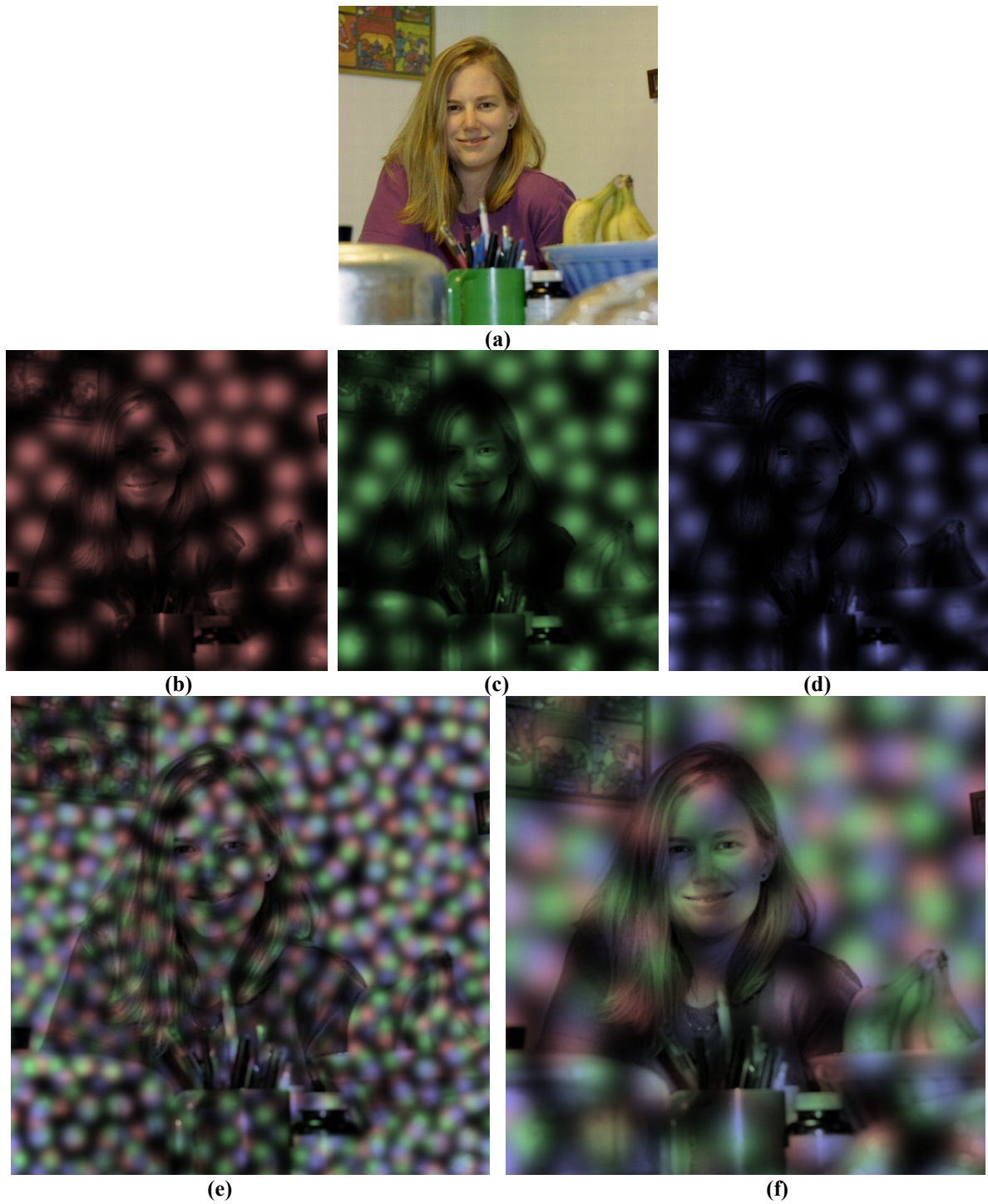


Figure 2.51: A photograph (a) is first split into RGB components and sampled with DDS alpha-blending (b-d). The alpha-blended layers are displayed with smaller spots in (e) and larger spots in (f). Notice that within the large spots the spatial details in the image can be seen and the image is recognizable.

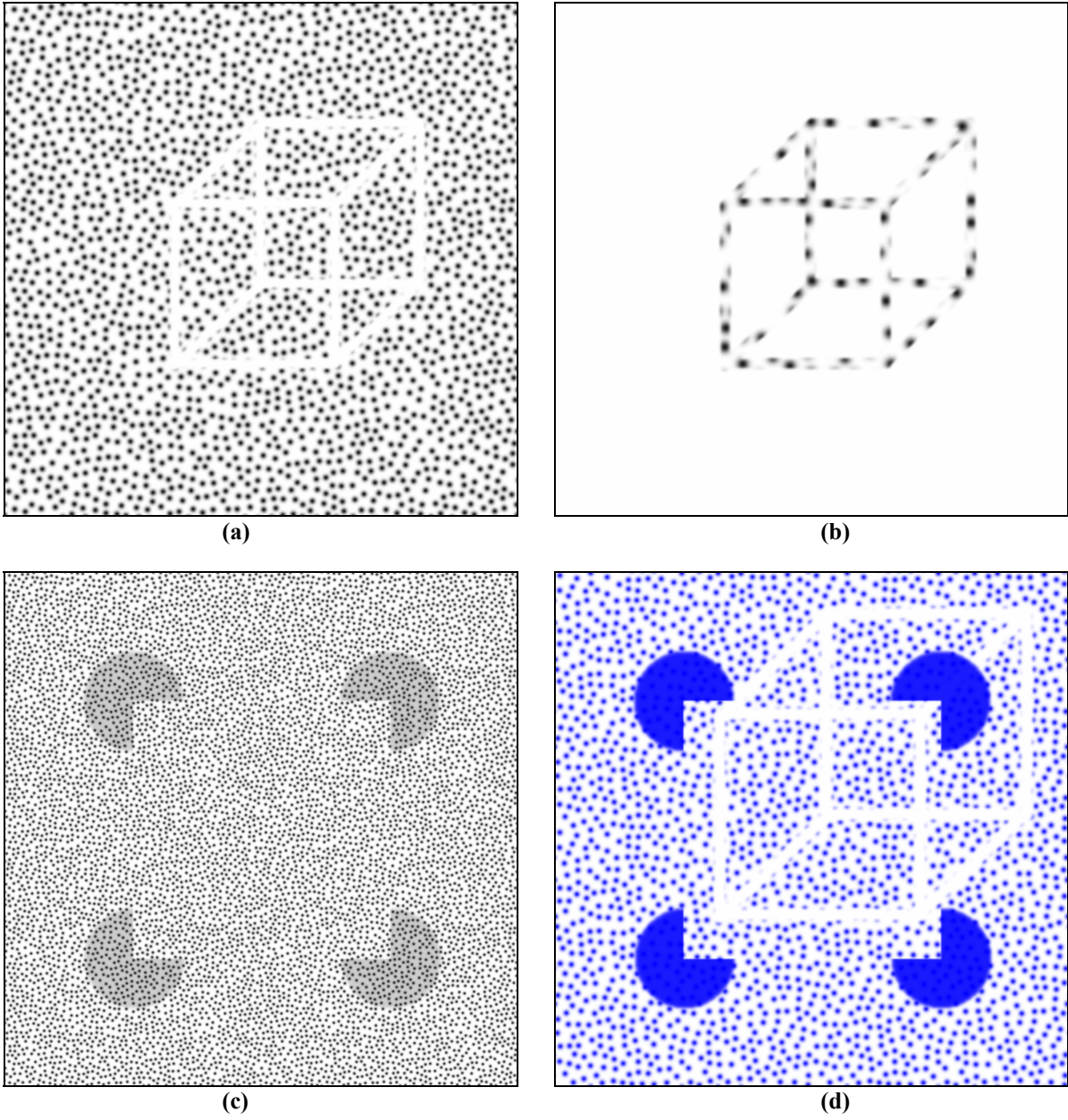
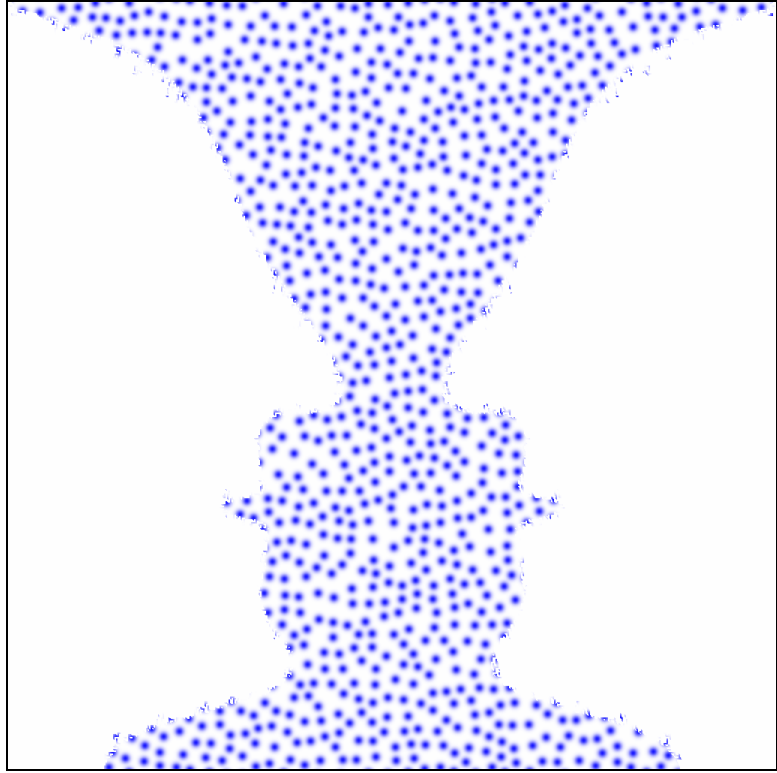
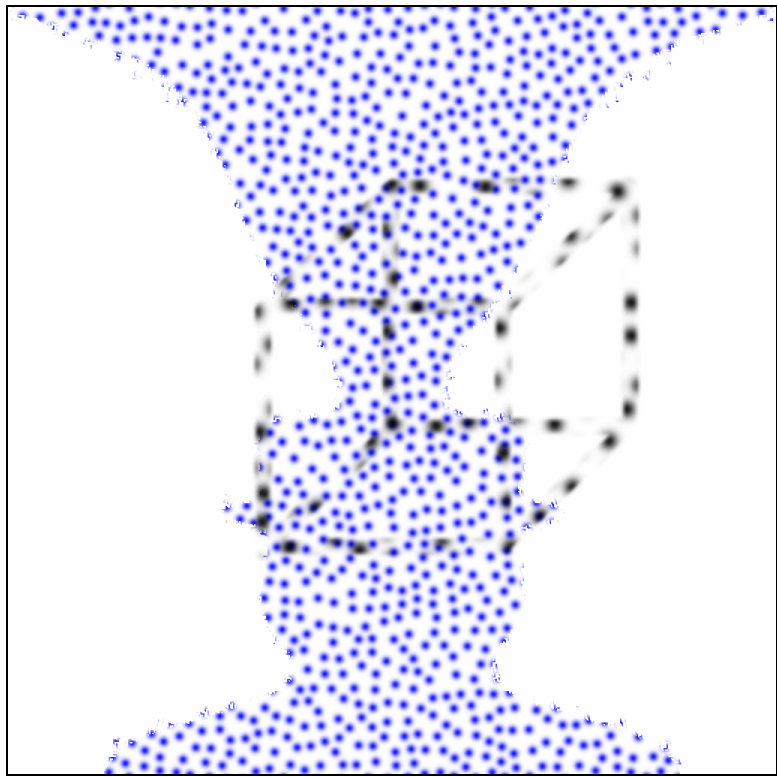


Figure 2.52: The Necker cube illusion (a) and (b); the magic square with a uniform field of spots on top in (c), despite the extra spots the magic square remains visible; the magic square and Necker cube combined in (d): both illusions persist despite being overlaid in a single image.



(a)



(b)

Figure 2.53: The face-vase illusion (a) and the face-vase illusion with the Necker cube from Figure 2.51 (b) overlaid on top.